9th ANKARA INTERNATIONAL AEROSPACE CONFERENCE **AIAC-2017-166**
20-22 September 2017 - METU, Ankara TURKEY

A STUDY ON CONTROLLABILITY OF AN AUGMENTED STABILITY FIGHTER AIRCRAFT

Dr. Ümit Kutluay[1], Assoc.Prof.Dr. Tayfun Çimen[2] and K. Gizem Parlak[3]
TAI
Ankara, Turkey

ABSTRACT

With advances in flight control systems, augmented stability aircraft became a reality, since they provide superior flight performance in terms of drag reduction. However, augmented stability aircraft need to be designed very carefully so that it remains controllable throughout its intended flight envelope. Thus, during conceptual and preliminary design phases, some guidelines are needed for the design to evolve in a controllable fashion. The relation between static stability and controllability is well discussed in the literature, and for fighter aircraft many studies are available. This paper investigates the "pitch stiffness coefficient" and its relation to longitudinal stability derivative and "pitch recovery moment" based allowable instability level.

DEFINITIONS & ABBREVIATIONS

a_{N_B}	Body normal acceleration component (along body negative z-axis direction)
$\bar{\bar{c}}$	Reference length (mean aerodynamic chord)
C_{L_α}	Lift curve slope
C_{m_α}	Longitudinal stability derivative
I_{YY}	Moment of inertia of aircraft around y axis
m	Aircraft mass
M	Mach number
M_α	Pitching moment slope – Dimensional stability derivative in longitudinal axis
M_y	Destabilizing moment in y axis
M_{yc}	Control moment in y axis
M_α/I_{YY}	Pitch Stiffness Coefficient – PSC
$\dot{q}$	Body pitch angular acceleration
S	Reference area of aircraft
T_2	Time to double amplitude
U_0	Speed in body x direction
V_T	True airspeed
α	Angle of attack

[1] Sr. Design Specialist, Air Vehicle Design, TF – X Group, Email: umit.kutluay@tai.com.tr
[2] Sr. Design Specialist, Flight Control System, TF - X Group, Email: tayfun.cimen@tai.com.tr
[3] Design Engineer, Flight Mechanics and Performance, Aircraft Group, Email: kezbangizem.parlak@tai.com.tr

η, δ_e	Actuator deflection angle
$\dot{\eta}$, $\dot{\delta}_e$	Actuator build up rate
ρ	Air density
τ_a	Actuator time constant
ζ_a	Actuator damping ratio
ω_a	Actuator natural frequency

INTRODUCTION

For fighter aircraft of the future, mission systems such as advanced radars, targeting systems, counter measures, as well as low signatures play a crucial role. However, like any aircraft, future fighters must have a well-balanced aerodynamic design which yields excellent handling qualities. From the flight performance point of view, an unstable basic airframe is essential. During airframe optimization for flight performance, a crucial question then arises: "how unstable can the aircraft be?" This question need to be answered by flight mechanics and flight control engineers. An unstable basic airframe will not be possible to fly without the continuous intervention of the Flight Control System (FCS). Thus, closed loop responses of the airframe and FCS need to be analyzed in detail to fully assess stability and controllability. This requires a high accuracy, medium to high fidelity aerodynamic model, actuator model and flight control algorithm. Also, for an air vehicle with a redundant set of control surfaces (such as differential flaps, all moving differential horizontal tail, low profile vertical tails, etc.) a control allocation/blending/prioritization algorithm is needed to be identified.

However, during early design stages of an air vehicle development program, the number of design alternatives is sometimes quite high for aerodynamics engineers to provide high accuracy and medium to high fidelity data. Furthermore, a need for alternative configurations to evolve rather quickly exists and, as a result, most of the design decisions are based on lower fidelity and accuracy models, analytical relations and rules of thumb. Thus, a very basic rule of thumb needs to be identified by flight mechanics and flight control engineers for the open-loop basic airframe instability level, so that aerodynamics and configuration development engineers can work on their designs knowing that it will be controllable in the end.

This paper presents a methodology that is devised in order to identify the basic stability constraint, which can be imposed as a constraint on air-vehicle sizing and design.

FLIGHT CONTROL SYSTEMS PERPECTIVE OF AIRCRAFT INSTABILITY LIMIT

The well-known short period approximation of the linearized equations of motion can be written as in Eq. 1 by considering

- Trimmed flight with wings level condition, and
- Worst-case analysis by neglecting dynamic damping derivatives in C_L and C_m ($C_{L_{\dot{\alpha}}}$, C_{L_q}, $C_{m_{\dot{\alpha}}}$, C_{m_q}) in order to stay on the "safe side" during conceptual design phase.

$$\left.\begin{aligned} \dot{\alpha} &= q - \frac{1}{mV_T}\left(L_\alpha \alpha + L_{\delta_e}\delta_e\right) \\ \dot{q} &= \frac{1}{I_{YY}}\left(M_\alpha \alpha + M_{\delta_e}\delta_e\right) \\ a_{N_B} &= \frac{1}{m}\left(L_\alpha \alpha + L_{\delta_e}\delta_e\right) \end{aligned}\right\} \quad \text{Eq. 1}$$

Dimensional stability derivatives in Eq. 1 are expressed as:

$$L_\alpha = \bar{q}SC_{Z_\alpha}, \qquad L_{\delta_e} = \bar{q}SC_{L_{\delta_e}}, \qquad M_\alpha = \bar{q}S\bar{\bar{c}}C_{m_\alpha}, \qquad M_{\delta_e} = \bar{q}S\bar{\bar{c}}C_{m_{\delta_e}} \quad \text{Eq. 2}$$

The following equation also follows easily from Eq. 1:

$$\left.\begin{aligned} \dot{a}_{N_B} &= \frac{1}{m}\left(L_\alpha q - \frac{L_\alpha}{V_T}a_{N_B} + L_{\delta_e}\dot{\delta}_e\right) \\ \dot{q} &= \frac{1}{I_{YY}}\left[\frac{M_\alpha}{L_\alpha}ma_{N_B} + \left(M_{\delta_e} - \frac{M_\alpha}{L_\alpha}L_{\delta_e}\right)\delta_e\right] \end{aligned}\right\} \quad \text{Eq. 3}$$

Actuator build up rate of Eq. 3 can be modeled as a first order linear differential equation (Eq. 4), so that the actuator dynamics is also included in the flight control algorithm design.

$$\dot{\delta}_e = \frac{1}{\tau_a}\left(\delta_{e_{com}} - \delta_e\right), \qquad \tau_a = \frac{1}{\zeta_a \omega_a} \quad \text{Eq. 4}$$

In Eq. 4, τ_a is the actuator time constant, ζ_a is the damping ratio, and ω_a is its natural frequency. Now the short period approximation can be represented in state-space form as Eq. 5 or equivalently as Eq. 6.

$$\underbrace{\begin{bmatrix} \dot{\alpha} \\ \dot{q} \\ \dot{\delta}_e \end{bmatrix}}_{\dot{x}} = \underbrace{\begin{bmatrix} -\dfrac{L_\alpha}{mV_T} & 1 & -\dfrac{L_{\delta_e}}{mV_T} \\ \dfrac{M_\alpha}{I_{YY}} & 0 & \dfrac{M_{\delta_e}}{I_{YY}} \\ 0 & 0 & -\zeta_a\omega_a \end{bmatrix}}_{A} \underbrace{\begin{bmatrix} \alpha \\ q \\ \delta_e \end{bmatrix}}_{x} + \underbrace{\begin{bmatrix} 0 \\ 0 \\ \zeta_a\omega_a \end{bmatrix}}_{B} \underbrace{\delta_{e_{com}}}_{u}$$

$$\underbrace{a_{N_B}}_{y} = \underbrace{\left[L_\alpha/m \quad 0 \quad L_{\delta_e}/m\right]}_{C} \underbrace{\begin{bmatrix} \alpha \\ q \\ \delta_e \end{bmatrix}}_{x} \quad \text{Eq. 5}$$

$$\underbrace{\begin{bmatrix}\dot{a}_{N_B}\\ \dot{q}\\ \dot{\delta}_e\end{bmatrix}}_{\dot{x}}=\underbrace{\begin{bmatrix}-\dfrac{L_\alpha}{mV_T} & \dfrac{L_\alpha}{m} & -\dfrac{L_{\delta_e}}{m}\zeta_a\omega_a\\ \dfrac{m}{I_{YY}}\dfrac{M_\alpha}{L_\alpha} & 0 & \dfrac{1}{I_{YY}}\left(M_{\delta_e}-\dfrac{M_\alpha}{L_\alpha}L_{\delta_e}\right)\\ 0 & 0 & -\zeta_a\omega_a\end{bmatrix}}_{A}\underbrace{\begin{bmatrix}a_{N_B}\\ q\\ \delta_e\end{bmatrix}}_{x}+\underbrace{\begin{bmatrix}\dfrac{L_{\delta_e}}{m}\zeta_a\omega_a\\ 0\\ \zeta_a\omega_a\end{bmatrix}}_{B}\underbrace{\delta_{e_{com}}}_{u} \qquad \text{Eq. 6}$$

$$\underbrace{a_{Z_B}}_{y}=\underbrace{\begin{bmatrix}1 & 0 & 0\end{bmatrix}}_{C}\underbrace{\begin{bmatrix}a_{Z_B}\\ q\\ \delta_e\end{bmatrix}}_{x}$$

Figure 1 shows the schematic of an integral (type 1) servomechanism control architecture. Here, the tracking command r, is the desired acceleration in body Z-axis direction, a_{Z_B}. Then the error, e is given by Eq. 7.

$$e = r - y \qquad \text{Eq. 7}$$

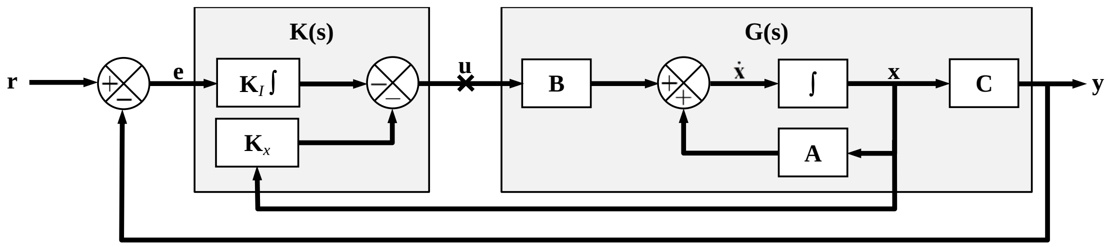

Figure 1: Integral servomechanism control architecture

Now an “augmented” state-space model can be constructed as in Eq. 8.

$$\dot{\mathbf{z}} = \tilde{\boldsymbol{A}}\mathbf{z} + \tilde{\mathbf{B}}u \qquad \text{Eq. 8}$$

with

$$u = \delta_{e_{com}}, \quad \mathbf{z} = \begin{bmatrix}\int e\\ \mathbf{x}\end{bmatrix}, \quad \tilde{\boldsymbol{A}} = \begin{bmatrix}0 & -\mathbf{C}\\ \mathbf{0}_{3\times1} & \mathbf{A}\end{bmatrix}, \quad \tilde{\mathbf{B}} = \begin{bmatrix}0\\ \mathbf{B}\end{bmatrix} \qquad \text{Eq. 9}$$

where $\mathbf{z} \in \mathbb{R}^4$ is the new augmented state vector, with $\tilde{\boldsymbol{A}} \in \mathbb{R}^{4\times4}$ and $\tilde{\mathbf{B}} \in \mathbb{R}^{4\times1}$. Using the augmented state vector $\mathbf{z}$, a full-state feedback control law is formed as in Eq. 10,

$$u = -\mathbf{K}\mathbf{z} \qquad \text{Eq. 10}$$

where $\mathbf{K} \in \mathbb{R}^{1\times4}$ is the state feedback gain matrix, which is partitioned in the same way as the augmented state vector $\mathbf{z}$ as in Eq. 11

$$u = [K_I \quad \mathbf{K}_x]$$ Eq. 11

with $K_I \in \mathbb{R}$ and $\mathbf{K}_x \in \mathbb{R}^{1\times 3}$, giving

$$u = -\mathbf{K}\mathbf{z} = -K_I \int e - \mathbf{K}_x \mathbf{x}$$ Eq. 12

This controller mechanization is frequently used in aerospace in the design of flight control systems. The integral servomechanism control architecture consists of two parts, with

- a servo tracking controller for command following, and
- a state feedback component for stabilization.

The desired integral control action on the tracking (command) error provides zero steady-state tracking (command following) error to a step input, through the use of the integrator and its gain $-K_I$, whereas the state feedback term $-\mathbf{K}_x\mathbf{x}$ enforces closed-loop stability of the system, requiring that the state vector $\mathbf{x}$ also be available for feedback, which would otherwise require an estimator such as a Kalman filter or observer.

By substitution, the closed-loop system dynamics becomes as in Eq. 13.

$$\begin{bmatrix} e \\ \dot{\mathbf{x}} \end{bmatrix} = \underbrace{\begin{bmatrix} 0 & -\mathbf{C} \\ \mathbf{B}K_I & \mathbf{A} - \mathbf{B}\mathbf{K}_x \end{bmatrix}}_{A_{CL}} \begin{bmatrix} \int e \\ \mathbf{x} \end{bmatrix} + \begin{bmatrix} 1 \\ \mathbf{0}_{3\times 1} \end{bmatrix} r$$ Eq. 13

Linear-quadratic (LQ) optimal control for command tracking is arguably the most widely used modern control design method in aerospace, due to its excellent properties of performance, robustness, and minimal control usage. When LQ optimal control theory is applied to the integral servomechanism control architecture given in Figure 1, the resulting closed-loop design using state feedback is guaranteed to be globally exponentially stable, forcing the regulated output to track the command signal $r = a_{Z_B}$ with zero steady-state error to a step input, additionally providing a control system design with predictable and robust performance.

For single-input systems, LQ optimal control ensures that the Nyquist locus never enters the unit circle centered about the $(-1, j0)$ point in the complex plane. This guarantees a gain margin (GM) of

$$GM = \left[\frac{1}{2}, +\infty\right] = [-6, +\infty]\ dB$$ Eq. 14

and a phase margin (PM) of at least 60°,

$$PM \geq 60°$$ Eq. 15

Such excellent frequency-domain properties of gain and phase margins make LQ optimal controllers very attractive in industrial applications (in addition to generating a minimizing control and command error, provided that the LQ optimal control problem is well posed).

The plant transfer function $G(s) \in \mathbb{R}$ of the integral servomechanism is given by

$$G(s) = \left(s\mathbf{I}_{4\times4} - \widetilde{\mathbf{A}}\right)^{-1}\widetilde{\mathbf{B}} \quad \text{Eq. 16}$$

The loop gain for this system, with controller transfer function $K(s) \in \mathbb{R}$, can be calculated by breaking the loop at the control generation point (plant input), indicated with a cross in Figure 1. With the loop break-point taken at the plant input, the loop gain of the integral servomechanism, represented by the loop-transfer function (LTF) $L(s) \in \mathbb{R}$, becomes

$$L(s) = K(s)G(s) \quad \text{Eq. 17}$$

Since it is a SISO system, the gain of the LTF is determined by computing the magnitude of this complex-valued transfer function versus frequency. Absolute stability is then easily established by examining the poles of the closed-loop transfer function of Eq. 18

$$T(s) = \frac{L(s)}{1 + L(s)} \quad \text{Eq. 18}$$

Equivalently, the eigenvalues of the closed-loop dynamics matrix $\mathbf{A}_{CL}$ can also be examined. For relative stability, on the other hand, classical stability margin analyses is pursued by manipulating the loop transfer function of the system to derive typical measures of GM and PM using frequency-response methods (such as Bode, Nichols and/or Nyquist). In addition, the PM leads to a time-delay margin (DM), corresponding to the minimum time delay at plant input such that the closed-loop system becomes unstable, which can be computed from

$$DM = \frac{PM}{\omega_c} \quad \text{Eq. 19}$$

where ω_c is the loop gain crossover frequency (LGCF), which corresponds to the frequency at which the magnitude of the LTF (at plant input) crosses 1 (0 dB), that is, $|L(j\omega)| = 1$.

FCS design of air vehicles dictates stringent requirements as robustness criteria, in the form of gain and phase margins, in that they must be simultaneously satisfied by ensuring that the loop transfer function $L(s)$ does not intersect (remains outside) the boundary depicted in Figure 2 and defined by (see, for example, [Mangold, 1990], [MIL-HDBK-1797, 1997] and [SAE AS 94900, 2007]):

- $\pm 6\ dB$ gain @ $\measuredangle L(j\omega) = -180°$ $(\min GM < -6\ dB$ and $\max GM > 6\ dB)$,
- $\pm 3\ dB$ gain @ $\measuredangle L(j\omega) = -145°$, and
- $PM \geq 45°$

These criteria must be met in the presence of total time delays (lags) due to:

- feedback sensors, such as air-data sensors and inertial measurement units (gyroscopes and accelerometers),
- flight control computer (computation, voting and transport delays)
- filtering (noise and structural coupling filters).

It is recommended that the total time-delay assumption due to these factors should be at least (>) 20 milliseconds, [Mangold, 1990].

To wrap up the ongoing discussion, the following model parameters are assumed for all flight control algorithm designs:

$$\frac{1}{m}L_\alpha = 500\,ms^{-2},\quad \frac{1}{m}L_{\delta_e} = 50\,ms^{-2},\quad \frac{1}{I_{YY}}M_{\delta_e} = -\frac{1}{I_{YY}}M_\alpha\left(\frac{\alpha}{\delta_e} = -1\right) \qquad \text{Eq. 20}$$

Three cases are now presented for different values of M_α/I_{YY} taken as

$$\frac{1}{I_{YY}}M_\alpha = \frac{1}{I_{YY}}\bar{q}S\bar{\bar{c}}C_{m_\alpha} = [15, 30, 45]\ s^{-2} \qquad \text{Eq. 21}$$

which directly affects air vehicle (in)stability. In each case, maximum allowable time-delay, $\max t_d$, the presence of which still satisfies the abovementioned robustness conditions, is determined. The results are graphically depicted in Figure 2. The limits achieved are summarized as follows:

- $M_\alpha/I_{YY} = 15\ s^{-2} \Longrightarrow \max t_d = 40\ ms$
- $M_\alpha/I_{YY} = 30\ s^{-2} \Longrightarrow \max t_d = 30\ ms$
- $M_\alpha/I_{YY} = 45\ s^{-2} \Longrightarrow \max t_d = 20\ ms$

All three cases satisfy $PM > 45°$, $\min GM < -6\ dB$ and $\max GM > 12\ dB$.

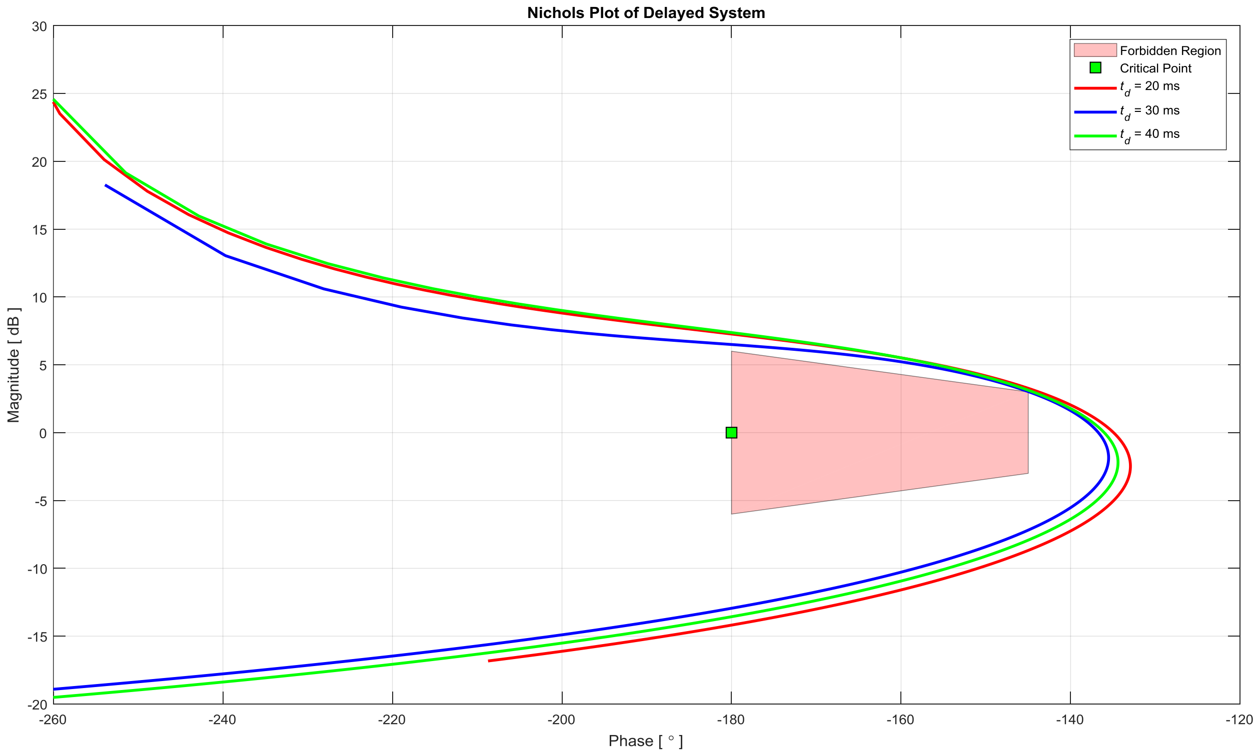

Figure 2: Nichols plot of the delayed system

As can be seen, maximum allowable time delay t_d is inversely proportional with M_α/I_{YY}, and the level of air-vehicle instability must be limited according to the time-delay budget for sensor hardware, FCS processing and structural coupling & noise filters.

FLIGHT MECHANICS PERPECTIVE OF AIRCRAFT INSTABILITY LIMIT

Once the basic requirement on instability level from a control design perspective is identified, the relation between longitudinal stability derivative and Mach number, altitude, angle of attack and moment of inertia of the aircraft can be sought. The quantity M_α/I_{YY} in Eq. 21, from now on referred as "pitch stiffness coefficient – PSC", can be re-written in following form of Eq. 22:

$$PSC = \frac{M_\alpha}{I_{YY}} = \frac{\rho V_T^2 S\bar{\bar{c}} C_{m_\alpha}}{2 I_{YY}} \qquad \text{Eq. 22}$$

Now, dimensionless longitudinal stability derivative C_{m_α} becomes:

$$C_{m_\alpha} = \frac{2\left(\frac{M_\alpha}{I_{YY}}\right) I_{yy}}{\rho V_T^2 S\bar{\bar{c}}} = \frac{2 \cdot \mathrm{PSC} \cdot I_{YY}}{\rho V_T^2 S\bar{\bar{c}}} \qquad \text{Eq. 23}$$

Now, for a given limited PSC value, Eq. 23 can be solved over Mach number and altitude to obtain the maximum allowed longitudinal stability derivative, depicted by the contour surface in Figure 3.

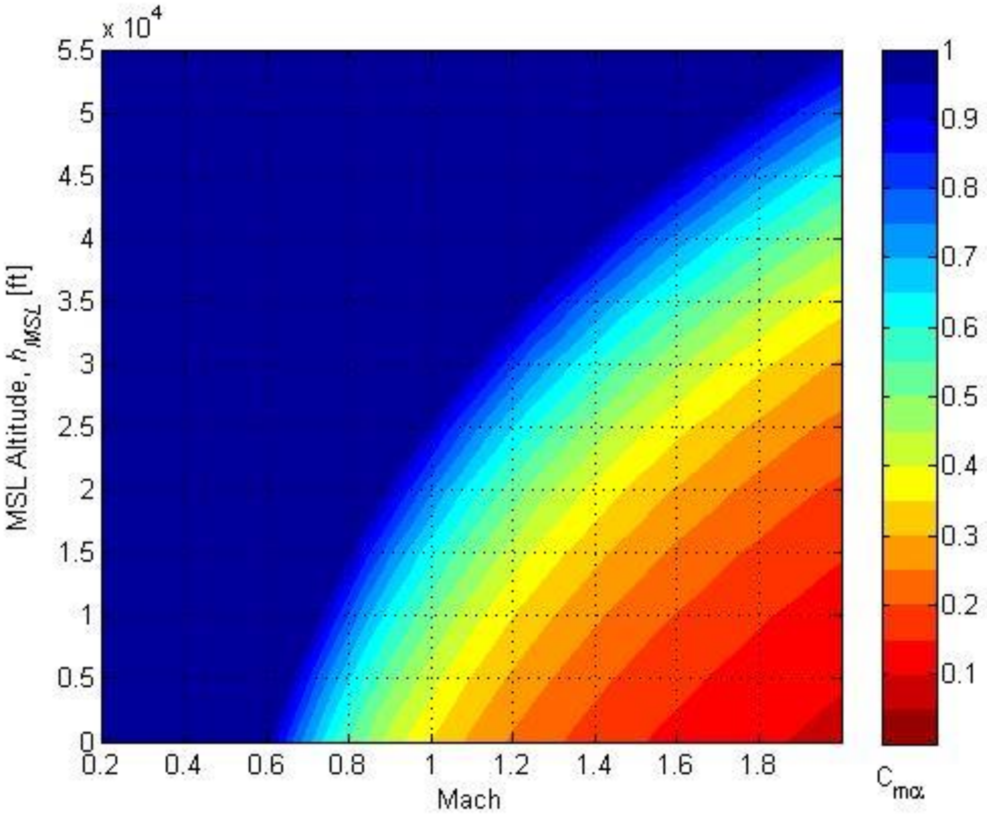

Figure 3: Variation of maximum allowable longitudinal stability derivative with Mach and altitude for PSC $\leq$ 45 s^{-2}

Note that, as dynamic pressure increases, the limit on the longitudinal stability derivative decreases. Also, lowering the PSC limit has a similar effect on maximum allowable longitudinal stability derivative value. Figure 3 demonstrates an interesting trend for longitudinal stability derivative. At first glance, it can be deduced that, even for a high level of instability, the aircraft can be controlled by FCS in low subsonic flight. However, the PSC metric, does not take into account the available control power, but it rather assumes that, the required control power is available at all times, Eq. 20. Since PSC is dimensional, it is affected from dynamic pressure, and the relative importance of longitudinal stability derivative seems to diminish with decreasing dynamic pressure. However, since the available control power also decreases with decreasing dynamic pressure, a very careful control power assessment analysis is needed for low subsonic flight conditions before reaching a conclusive remark.

Of all the dynamic stability parameters, time to double amplitude is of significant importance, because it provides crucial information about the controllability of aircraft, [Mangold, 1990]. Time to double amplitude, T_2, is the time required for a controls-fixed aircraft, to double its angle of attack in response to a gust input. Figure 4 shows a simplified plot for the relation of T_2 with controllability. Once an unstable aircraft flying at wings level trimmed flight is suddenly disturbed by a gust, a destabilizing moment starts to build up. It is essential to counteract this moment by stabilizing control input. However, total delay in FCS and actuator, actuator build up rate ($M_{\dot{\eta}}$), as well as maximum attainable control moment all play a crucial role in stabilizing the aircraft.

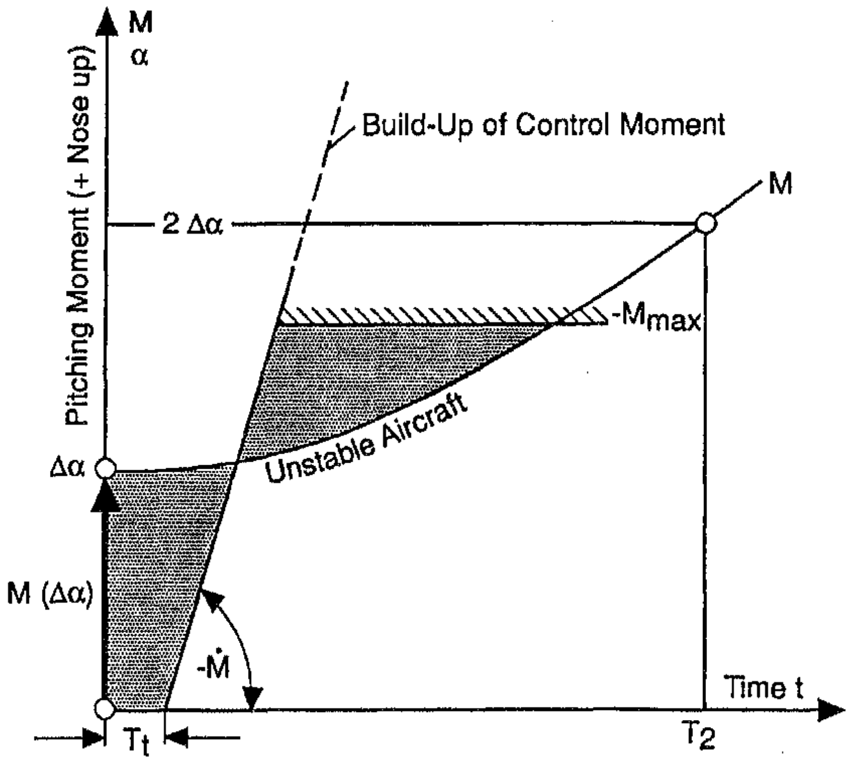

Figure 4: Allowable instability level schematic [Mangold, 1990].

To carry out the control-fixed T_2 analysis over the entire flight envelope (M and altitude), short-period approximation of longitudinal equation of motion given in Eq. 1 can be re-written as Eq. 24, [Pamadi, 1998], with one additional assumption:

- The magnitude of gust depends on gust penetration speed and flight altitude, [MIL-HDBK-1797, 1997].

$$\begin{bmatrix} \Delta\dot{\alpha} \\ \dot{q} \end{bmatrix} = \begin{bmatrix} \frac{C_{L_\alpha}\rho U_0 S}{2m} & 1 \\ \frac{2C_{m_\alpha}\rho U^2 S\bar{\bar{c}}}{I_{YY}} & 0 \end{bmatrix} \begin{bmatrix} \Delta\alpha \\ q \end{bmatrix} + \begin{bmatrix} \frac{C_{L_{\delta_e}}\rho U_0 S}{2m} \\ \frac{2C_{m_{\delta_e}}\rho U^2 S\bar{\bar{c}}}{I_{YY}} \end{bmatrix} \Delta\delta_e \quad \text{Eq. 24}$$

The aerodynamic data is generated with NS CFD simulations for the conditions given in Table 1. A polynomial model is fit on the aerodynamic database to obtain a global model.

Table 1: CFD Solution Nodes

Mach	AoA [°]	Elevator deflection [°]
0.3	[-10, -5, 0, 5, 10, 15, 20]	[-25, -15, 0, 15, 25]
0.8		
0.9		
1.2		
1.4		

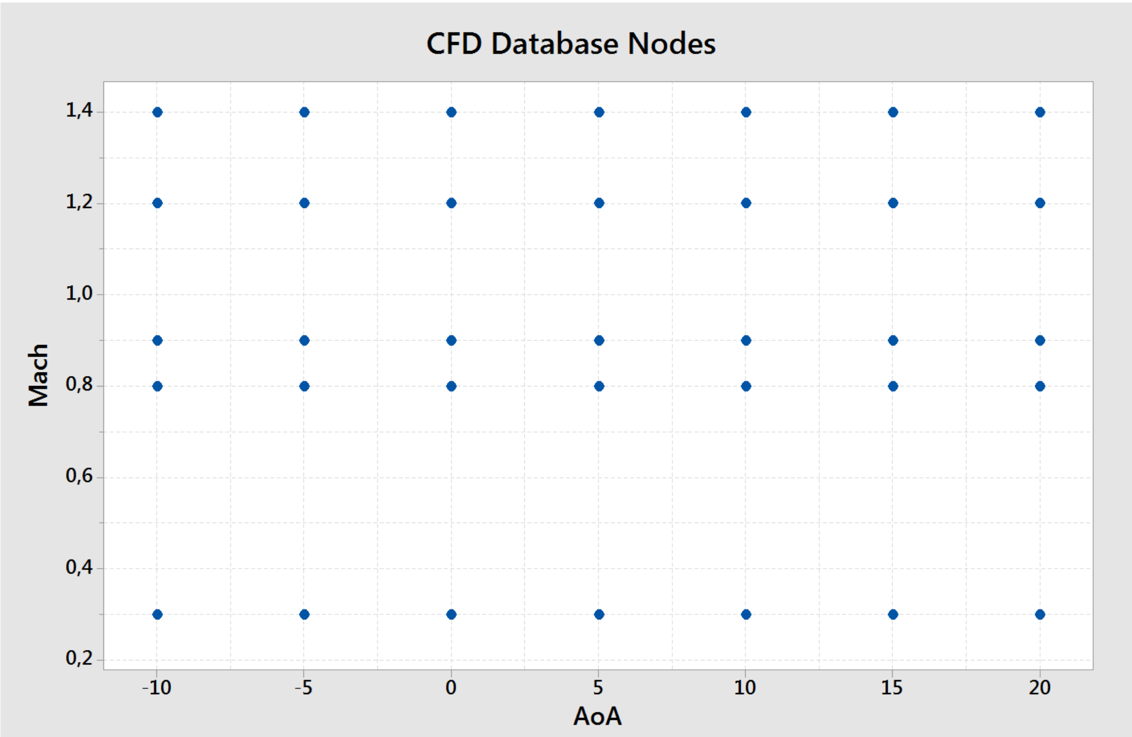

Figure 5: Nodes of the aerodynamic database

Aerodynamics is modeled as a polynomial function of Mach, angle of attack and elevator deflection angle. Although the statistics of the models have some deficiencies (Figure 6 – Figure 8), they are still considered as feasible models for the purpose of this study.

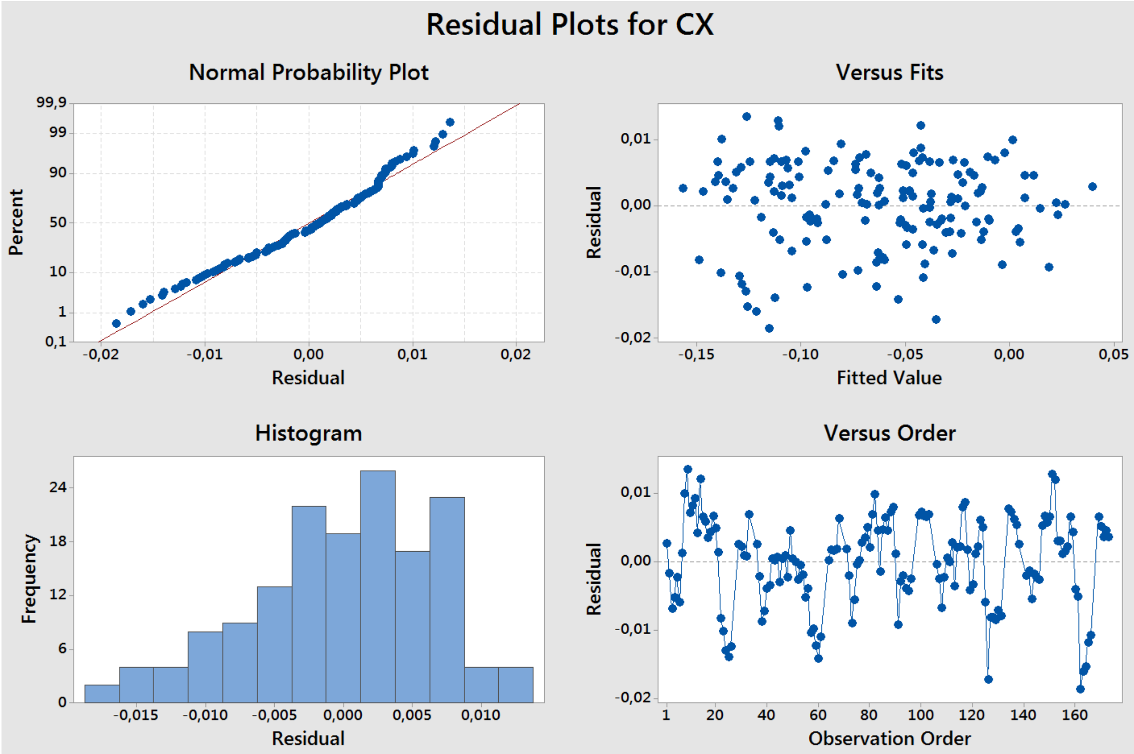

Figure 6: Model fit statistics for C_X

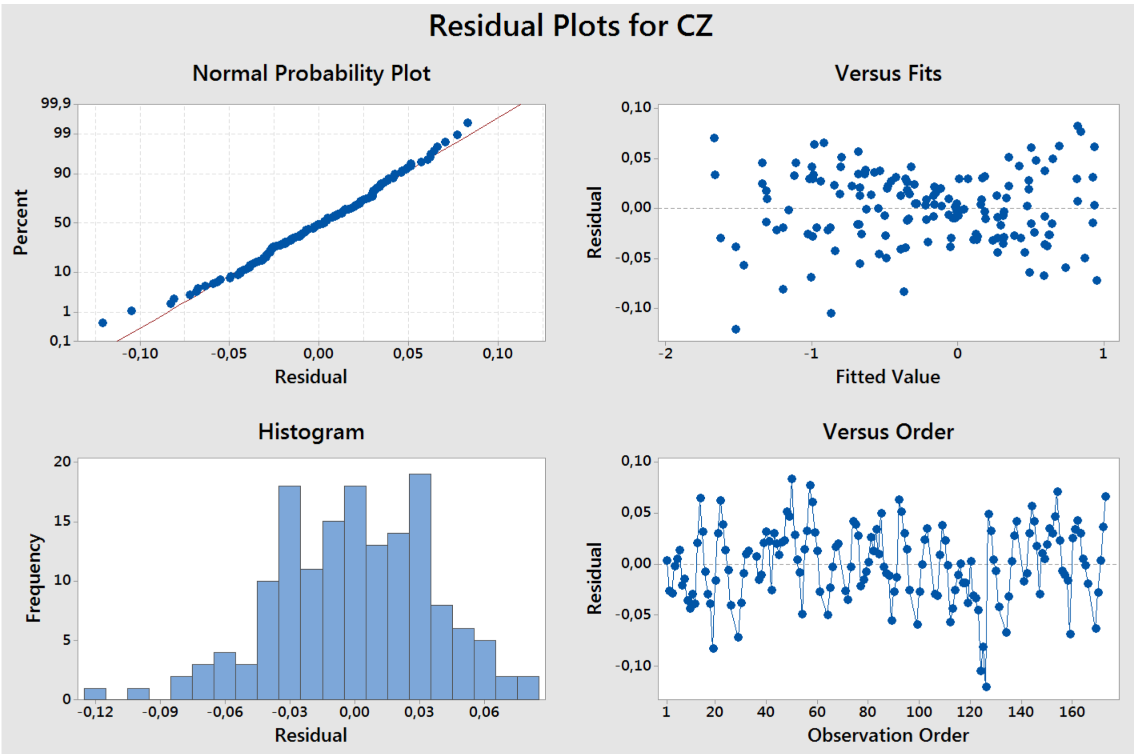

Figure 7: Model fit statistics for C_Z

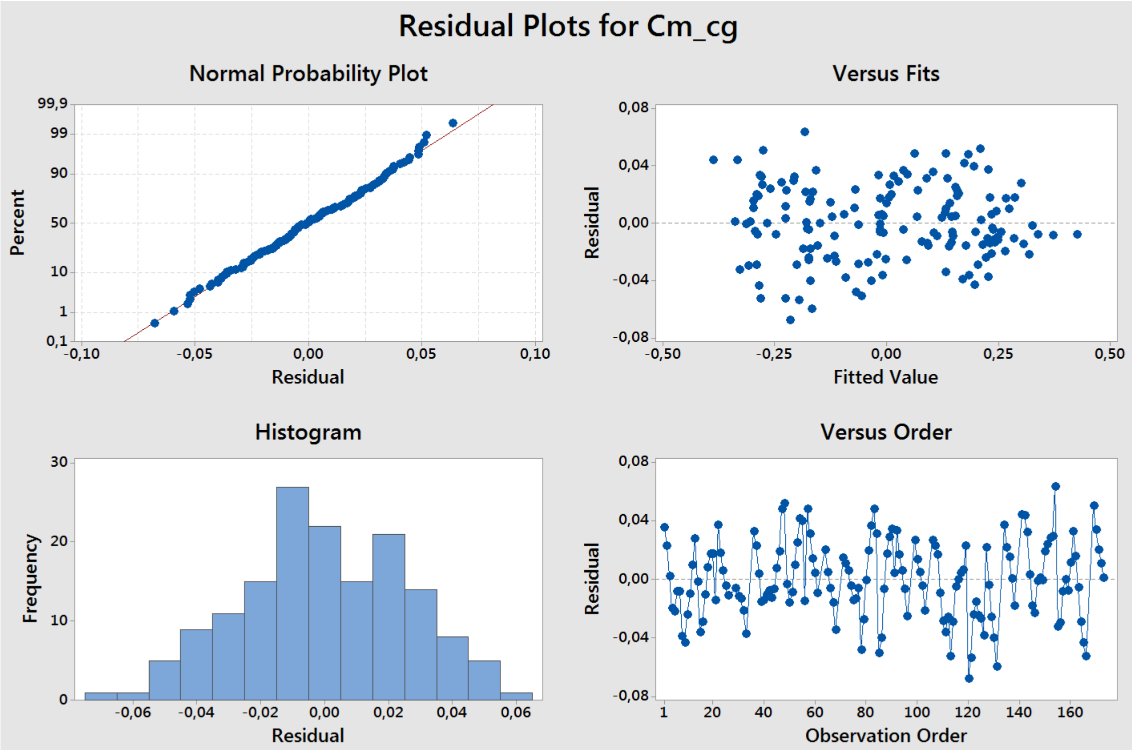

Figure 8: Model fit statistics for C_m

The entire flight envelope in Mach and altitude is swept and for each trimmed flight condition (trim angle of attack corresponding to the selected Mach and altitude node), severe gusts [MIL-HDBK-1797, 1997] are applied and the control surfaces fixed response of the simplified short-period mode is obtained. Actuator dynamics is modeled with a delay time and maximum rate, and it is assumed that the pilot applies full control power, as soon as the gust ends. Figure 9 and Figure 10 show the instability level schematic for uncontrollable and controllable cases, respectively. One important thing to notice is the T_2 values of uncontrollable and controllable cases; uncontrollable case has a higher T_2 than the controllable one! The root reason of this behavior is something to be explored, but it could very well be due to the low fidelity nature of aerodynamic database.

To better capture the extent of controllable and uncontrollable flight regimes, a simple metric is devised to compare the attainable control power with destabilizing moment induced by external disturbance. Named as “Control Power Metric – CPM”, the mathematical expression is provided in Eq. 25, where $M_{yc}(t)$ denotes the control moment and $M_y(t)$ is the destabilizing moment in y axis. It is obvious that, for a controllable unstable aircraft, CPM must be greater than zero for all flight cases.

$$CPM = \frac{\int_{T_d}^{T_2} M_{yc}(t)dt - \int_0^{T_2} M_y(t)dt}{\int_{T_d}^{T_2} M_{yc}(t)dt} > 0 \qquad \text{Eq. 25}$$

Figure 11 and Figure 12 show CPM and variation of longitudinal stability derivative with angle of attack and Mach number for a generic augmented stability fighter aircraft with conventional wing-tail configuration. CPM value falls below zero around 0.6 M, almost regardless of altitude. When the contour plot of Figure 12 is examined, it is seen that longitudinal stability derivative exceeds 0.4 value around 0.6 M and stays above 0.4 for all M < 0.6.

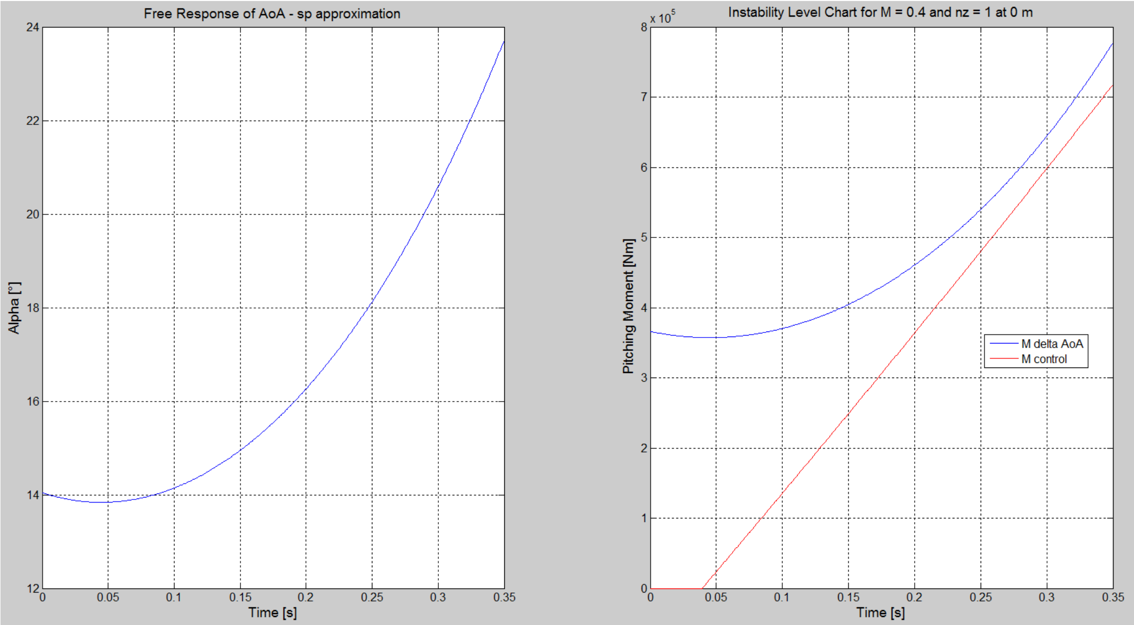

Figure 9: Uncontrollable case plot

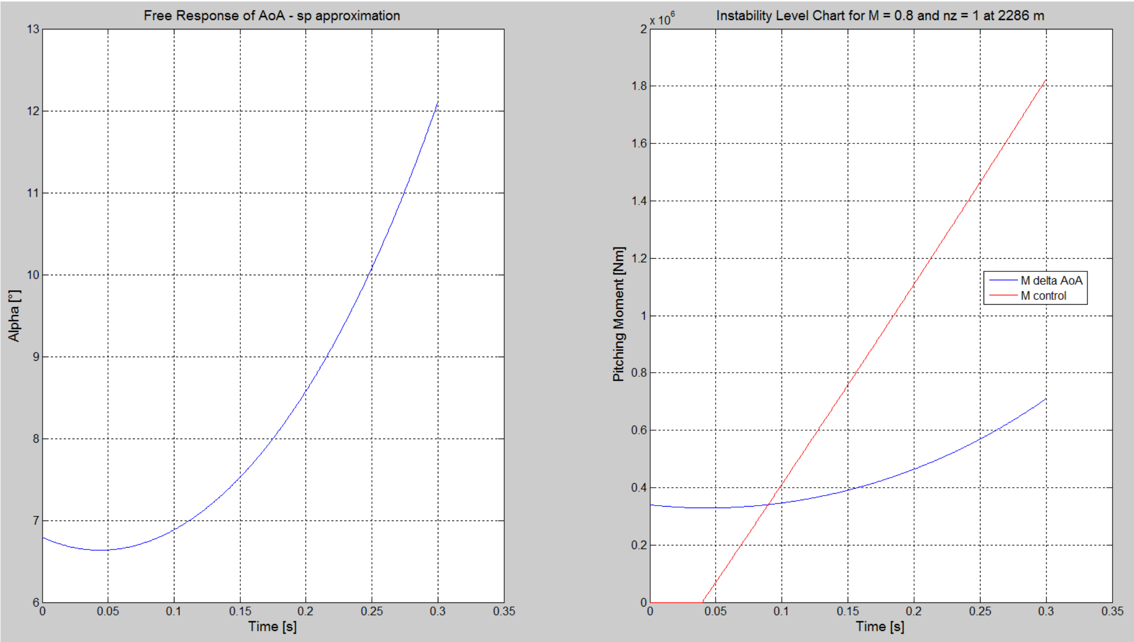

Figure 10: Controllable case plot

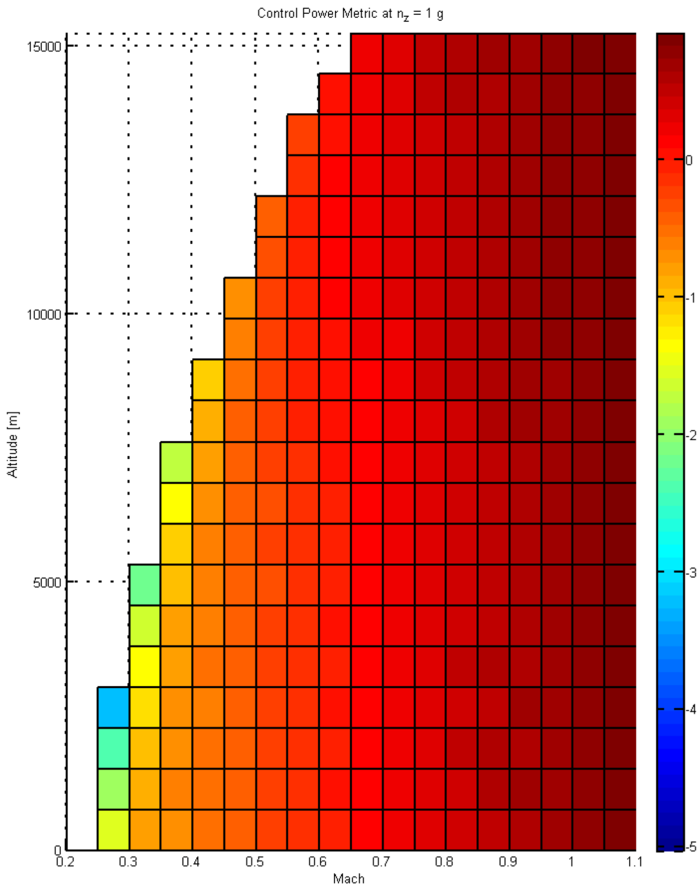

Figure 11: CPM Variation with Altitude and Mach

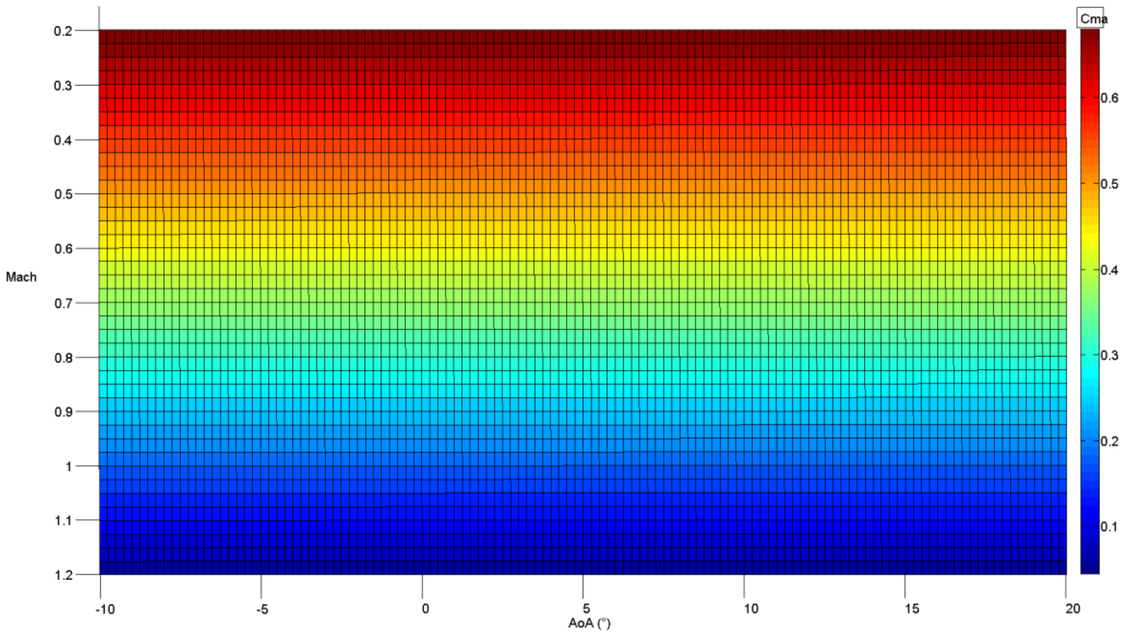

Figure 12: Longitudinal stability derivative variation with Mach and angle of attack

CONCLUSION

This paper demonstrated the applicability of longitudinal controllability methods found in the literature to unstable basic airframe of an aircraft. From a flight control engineering perspective, PSC seems to be most important parameter in stating an allowable instability level in conceptual and early preliminary design. The longitudinal stability derivative values corresponding to a fixed PSC limit is investigated over the flight envelope and it is seen that, dynamic pressure has dominance over the limiting values. However, without the inclusion of available control power assessment, pure PSC based instability level limitation might be somewhat incomplete. So, allowable instability level schematic is utilized and the findings are in parallel to the values suggested in literature for longitudinal stability derivative.

References

Mangold P. (1990), Flying Qualities, Integration of Handling Quality Aspects into the Aerodynamic Design of Modern Unstable Fighters, AGARD Conference Proceedings No: 508

MIL-HDBK-1797 Flying Qualities of Piloted Aircraft 1997

Pamadi B.N. (1998), Performance, Stability, Dynamics and Control of Airplanes, AIAA Education Series

SAE AS 94900 (2007), Aerospace - Flight Control Systems - Design, Installation and Test of Piloted Military Aircraft, General Specification For